JOURNAL OF GUIDANCE, CONTROL, AND DYNAMICS
Vol. 32, No. 5, September–October 2009

Propellantless Stationkeeping at Enceladus via the Electromagnetic Lorentz Force

Joseph W. Gangestad,* George E. Pollock,* and James M. Longuski†
Purdue University, West Lafayette, Indiana 47907-2045

DOI: 10.2514/1.42769

An introduction to the dynamics of an electrostatically charged spacecraft in two- and three-body regimes is presented, with particular attention to a promising application at Enceladus. Equilibrium solutions to the equations of motion are found, and the stability of the orbits assessed. The perturbative Lorentz force, produced by interaction of the spacecraft with a planetary magnetic field, creates trajectories that are not possible with Newtonian gravity alone. A heuristic, analytical control law with single-variable scalar feedback allows a charged spacecraft to remain near the collinear Lagrange points on either side of Enceladus. The mission feasibility depends on the charge requirement, which is primarily affected by the navigational accuracy. For example, an insertion error into the cis-Enceladus Lagrange point of 10 km in position and 1 m/s in velocity requires a specific charge of approximately 0.05 C/kg. Other significant gravitating bodies in the Saturnian system do not have a substantive effect on the charge requirements or on the stability. Given a sufficiently accurate insertion, a charged spacecraft could maintain station near Enceladus without propellant.

Nomenclature

$\mathbf{A}$	=	magnetic vector potential, T · km
A	=	tether cross-sectional area, mm^2
$\mathbf{a}$	=	acceleration vector at Enceladus, m/s^2
a	=	acceleration at Enceladus, m/s^2
$\mathbf{B}$	=	magnetic field vector, T
B_0	=	magnetic moment, T · km^3
$\mathbf{E}$	=	planetary electric field vector, km/(s^{2}C)
$\mathbf{F}_g$	=	specific gravitational force vector, km/s^2
$\mathbf{F}_L$	=	specific Lorentz force vector, km/s^2
$\mathbf{I}$	=	tether current vector, C/s
I	=	tether current, C/s
$\mathcal{L}$	=	Lagrangian, km^2/s^2
l	=	length of tether, km
M	=	generalized specific angular momentum, km^2/s
m_{tot}	=	total mass of tether spacecraft, kg
P	=	tether power, W
q	=	specific charge, C/kg
R	=	radius of reference circular orbit, km
$\mathbf{r}$	=	position vector, km
$\hat{\mathbf{r}}$	=	radial unit vector
r	=	radial coordinate, km
r_E	=	orbital radius of Enceladus, km
U_{eff}	=	effective potential, km^2/s^2
u_k	=	roots of the effective potential ($k = 1, 2, 3$), km^{-1}
V	=	tether voltage, V
$\mathbf{v}$	=	inertial velocity, km/s
$\mathbf{v}_{\text{rel}}$	=	velocity relative to magnetic field, km/s
Z	=	resistance of tether ribbon, Ω
α	=	tuning parameter of control law
δv_i	=	perturbation of velocity in the i-coordinate direction, km/s
$\hat{\theta}$	=	polar unit vector
θ	=	polar coordinate, rad
μ	=	gravitational parameter, km^3/s^2
μ_E	=	gravitational parameter of Enceladus, km^3/s^2
μ_S	=	gravitational parameter of Saturn, km^3/s^2
$\hat{\phi}$	=	azimuthal unit vector
ϕ	=	azimuthal coordinate, rad
ρ	=	resistivity of tether material, Ω · m
Ω	=	orbital angular velocity of Enceladus, rad/s
ω	=	planetary rotational angular velocity, rad/s
ω_S	=	rotational angular velocity of Saturn, rad/s

Received 5 January 2009; revision received 18 May 2009; accepted for publication 29 May 2009.

*Ph.D. Candidate, School of Aeronautics and Astronautics, 701 West Stadium Avenue. Student Member AIAA.

†Professor, School of Aeronautics and Astronautics, 701 West Stadium Avenue. Associate Fellow AIAA.

Introduction

THE exploration of small bodies in orbit about large primaries by its nature requires frequent stationkeeping maneuvers. However, the quantity of onboard propellant constrains the duration of these missions. To enable a broader range of targets for future science missions, it may be advantageous to consider propellantless methods of orbit control.

This paper considers a nascent propellantless vehicle, which we shall call a Lorentz spacecraft, that generates an electrostatic charge on its surface, inducing a Lorentz force on the spacecraft as it travels through a planetary magnetic field. Active modulation of the surface charge allows the spacecraft to perform maneuvers without propellant. The dynamics of small charged particles in space (i.e., dust) has long been a subject of interest in physics and astronomy [1–3], but the introduction of control for a massive charged particle (i.e., a spacecraft) constitutes a new engineering problem.

A Lorentz spacecraft is propelled according to the same physics as an electrodynamic tether but has the potential for compact construction, so that the spacecraft may be modeled as a charged point mass. This particle treatment decouples the vehicle's attitude dynamics and orbital mechanics, which is not always possible with a tether, and opens up many potent propellantless applications, including low-Earth geosynchronous orbit [4], inclination change [5], and planetary escape and capture [6].

The feasibility of realizing a Lorentz spacecraft remains an open question, especially in the case of specific charges greater than a few hundredths of a coulomb per kilogram. The physical challenges were first laid out by Peck [7], who proposed a variety of solutions to the problem of charge generation and storage, including van de Graaff generators, radioactive isotopes, biological sources, and carbon nanotechnology. The development of a Lorentz spacecraft test bed is ongoing [8,9]. It is generally accepted that a specific charge of 0.001–0.01 C/kg is near-term feasible with a concerted research

effort, and so we restrict our applications (in particular for observation of Enceladus) to these orders of magnitude. Overcoming the challenges of arcing, charge storage, and charge generation for specific charges greater than 0.1 C/kg lies in the future. At the end of this paper, we provide a brief comparison of the performance of Lorentz spacecraft against electrodynamic tethers and low-thrust propulsion technology.

Assumptions

To make the analysis tractable we impose several assumptions, which apply throughout.

1) The Lorentz spacecraft may be treated as a charged point mass in space.

2) Gravity and the Lorentz force are the only forces acting on the spacecraft. All other perturbing forces (e.g., planetary oblateness and radiation pressure) are neglected. For a first-order analysis, these perturbations may be ignored, as they will be several orders of magnitude weaker than gravity and the artificially enhanced Lorentz force [10].

3) A planetary magnetic field may be modeled as that of a perfect dipole at the planet's center, and there are no electric fields or currents local to the planet. (Higher-fidelity analyses should take into account other harmonics and multipole effects, which may be significant [11].)

4) The planetary magnetic dipole is aligned with the planet's rotation axis and corotates with the planet. This assumption is reasonable for Saturn, whose magnetic dipole tilt is less than 1 deg [11]. (The effect of a small dipole tilt is negligible [4].)

5) The Lorentz spacecraft may modulate its electrostatic charge at high bandwidth and may create both positive and negative charges. The rise time of spacecraft charging is on the order of milliseconds [12], much shorter than the needs of applications presented here.

We also note that, throughout this paper, all physical quantities referred to are understood to be specific (e.g., a reference to the spacecraft's angular momentum implies its specific angular momentum).

Dynamics

The force due to gravity is modeled by an inverse-square field,

$$\mathbf{F}_g = -\mu\mathbf{r}/r^3 \tag{1}$$

Gravity is the dominant force in this treatment, ensuring that orbits continue to appear Newtonian in form plus a perturbation from the Lorentz force. The Lorentz force is given by

$$\mathbf{F}_L = q(\mathbf{E} + \mathbf{v}_{\text{rel}} \times \mathbf{B}) \tag{2}$$

where $\mathbf{v}_{\text{rel}}$ is the velocity relative to the magnetic field, which is related to the inertial velocity by

$$\mathbf{v}_{\text{rel}} = \mathbf{v} - \omega \times \mathbf{r} \tag{3}$$

Because we assume there are no local currents (i.e., $\mathbf{E} = 0$), the Lorentz force on the spacecraft is due solely to the magnetic field. The magnetic field of a perfect dipole may be described by its vector potential

$$\mathbf{A} = (B_0 \sin\theta/r^2)\hat{\phi} \tag{4}$$

whence the magnetic field ($\nabla \times \mathbf{A}$) is given by [13]

$$\mathbf{B} = (B_0/r^3)(2\cos\theta\hat{\mathbf{r}} + \sin\theta\hat{\theta}) \tag{5}$$

where r is measured from the center of the planet and dipole, and θ is the angle measured from the axis of planetary rotation, as shown in Fig. 1. The unit vector $\hat{\phi}$ points in the direction of planetary rotation, completing the set of spherical polar coordinates. The x, y, and z coordinates in Fig. 1 are used for reference in defining the spherical coordinates. The planet and dipole rotate about the z axis, and, because the dipole is axially symmetric, the inertial orientation of the x and y axes is arbitrary.

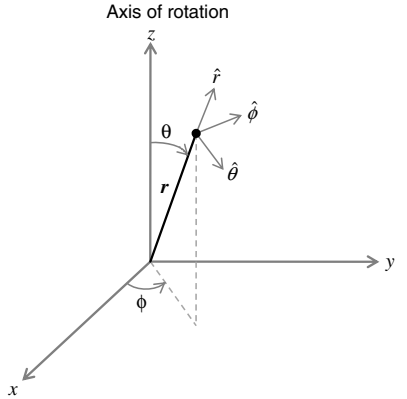

Fig. 1 Spherical coordinate system and unit vectors used in this analysis, with origin at the center of the planet and dipole.

For a massive charged particle (the Lorentz spacecraft), we pursue a Lagrangian formulation to derive the equations of motion. Using $-\mathbf{v}_{\text{rel}} \cdot \mathbf{A}$ for the velocity-dependent potential in the Lagrangian [14], we have

$$\mathcal{L} = (\tfrac{1}{2})(\dot{r}^2 + r^2\dot{\theta}^2 + r^2\dot{\phi}^2\sin^2\theta) + \mu/r + q\mathbf{v}_{\text{rel}} \cdot \mathbf{A} \tag{6}$$

where insertion of Eqs. (3) and (4) yields

$$\mathcal{L} = (\tfrac{1}{2})(\dot{r}^2 + r^2\dot{\theta}^2 + r^2\dot{\phi}^2\sin^2\theta) + \mu/r + (qB_0\sin^2\theta/r)(\dot{\phi} - \omega) \tag{7}$$

Application of the Lagrange equations to Eq. (7) produces the equations of motion

$$\ddot{r} - r\dot{\theta}^2 - r\dot{\phi}^2\sin^2\theta + \mu/r^2 + (qB_0\sin^2\theta/r^2)(\dot{\phi} - \omega) = 0 \tag{8}$$

$$r\ddot{\theta} + 2\dot{r}\,\dot{\theta} - r\dot{\theta}^2\sin\theta\cos\theta - 2(qB_0\sin\theta\cos\theta/r^2)(\dot{\phi} - \omega) = 0 \tag{9}$$

$$\frac{\mathrm{d}}{\mathrm{d}t}[r^2\dot{\phi}\sin^2\theta + qB_0(\sin^2\theta/r)] = 0 \tag{10}$$

as also found by Streetman and Peck [4]. (This result is a special case of the tilted dipole equations of motion, which we derived in an earlier work [5] by a similar approach.)

Throughout this paper, we consider only equatorial orbits ($\theta = \pi/2$). We observe immediately that a circular ($\dot{r} = 0$), synchronous ($\dot{\phi} = \omega$) orbit satisfies these equations of motion. Because we have assumed the magnetic field rotates with the planet, a synchronous orbit (occurring at one fixed synchronous radius) has no velocity relative to the magnetic field, eliminating the Lorentz force and leaving a purely gravitational orbit. A particular solution to Eqs. (8–10) permits a circular orbit of arbitrary radius R subject to the condition

$$\dot{\phi} = \frac{1}{2R}\left[-\frac{qB_0}{R^2} \pm \sqrt{\frac{q^2B_0^2}{R^4} + 4\frac{\mu}{R}\left(1 + \frac{qB_0\omega}{\mu}\right)}\right] \tag{11}$$

which reduces to the mean motion when $q = 0$. The two roots correspond to prograde and retrograde orbits. The spacecraft may travel at an arbitrary velocity in this circular orbit, given the correct specific charge q to satisfy Eq. (11). Solving Eq. (11) for q gives

$$q = \frac{R^3\dot{\phi}^2 - \mu}{B_0(\dot{\phi} - \omega)} \tag{12}$$

From the set of parameters $\{q, R, \dot{\phi}\}$, which can completely define a circular equatorial orbit, we may choose any two, with the third

determined by Eq. (11) or Eq. (12). A multibody analogue of Eq. (12) will be essential later in the development of a control law for maintaining an orbit near Enceladus.

Momentum in the ϕ direction (which, for an equatorial orbit, is the entire orbital angular momentum) is conserved, as ϕ is an ignorable coordinate in this system. Defining the constant M to denote the generalized angular momentum associated with ϕ, we may write

$$\dot{\phi} = (M/\sin^2\theta - qB_0/r)/r^2 \tag{13}$$

For equatorial orbits, we set $\theta = \pi/2$ and Eq. (13) becomes

$$\dot{\phi} = (M - qB_0/r)/r^2 \tag{14}$$

When the Lorentz force is removed ($q = 0$), Eq. (14) reduces to the familiar purely gravitational form, where $M = h$, the angular momentum.

Inserting Eq. (14) into Eq. (8), only the r coordinate remains in the equation of motion,

$$\ddot{r} + \frac{\mu}{r^2}\left(1 - \frac{qB_0\omega}{\mu}\right) - \frac{M^2}{r^3} + \frac{3qB_0M}{r^4} - \frac{2q^2B_0^2}{r^5} = 0 \tag{15}$$

We define an effective potential that is quartic in $1/r$ for these equatorial orbits U_{eff}, where

$$U_{\text{eff}} = -\frac{\mu}{r}\left(1 - \frac{qB_0\omega}{\mu}\right) + \frac{M^2}{2r^2} - \frac{qB_0M}{r^3} + \frac{q^2B_0^2}{2r^4} \tag{16}$$

so that Eq. (15) may be written as $\ddot{r} + \partial U_{\text{eff}}/\partial r = 0$.

The quartic effective potential of Eq. (16) gives rise to as many as three extrema, including two local minima. Particular combinations of angular momentum and energy can create a potential that allows for two stable circular orbits at different radii but each with the same angular momentum and specific charge. Furthermore, we note that the quartic term in Eq. (16) is always positive, forcing a positive asymptote at small r and ensuring that a particle in the system can never reach $r = 0$. A positive asymptote accompanied by local extrema from the quartic expression (which requires one, two, or three extrema) implies that there must always exist at least one minimum. This system, including both gravity and the Lorentz force, distinguishes itself from the purely Lorentz case, for which no stable circular orbits exist [15].

To briefly investigate the extrema of the effective potential, we make a change of variables $1/r = u$, so that Eq. (16) becomes

$$U_{\text{eff}} = -\mu(1 - qB_0\omega/\mu)u + (M^2/2)u^2 - qB_0Mu^3 + (q^2B_0^2/2)u^4 \tag{17}$$

The stationary points may be found by taking the derivative

$$\mathrm{d}U_{\text{eff}}/\mathrm{d}u = -\mu(1 - qB_0\omega/\mu) + M^2u - 3qB_0Mu^2 + 2q^2B_0^2u^3 = 0 \tag{18}$$

and solving for u.

It is possible to solve for the three roots of the cubic Eq. (18) analytically by means of the Chebyshev cube root. We define

$$a = -3M/2qB_0 \tag{19}$$

$$p = (1/12)(M/qB_0)^2 \tag{20}$$

$$t = 12\sqrt{3}(qB_0\mu/M^3)(1 - qB_0\omega/\mu) \tag{21}$$

Then, the three roots of the cubic $\{u_0, u_1, u_2\}$ are

$$u_0 = \sqrt{p}C_{1/3}(t) - a/3 \tag{22}$$

$$u_1 = -\sqrt{p}C_{1/3}(-t) - a/3 \tag{23}$$

$$u_2 = -u_0 - u_1 - a \tag{24}$$

where the Chebyshev cube root is given by $C_{1/3}(t) = 2\cos[\arccos(t/2)/3]$. If $-2 \le t \le 2$, there are three real roots. For example, for orbits at twice the planetary radius and a constant specific charge of 0.1 C/kg, the highest practical specific charge considered here, the values of t are approximately -0.02 and 0.04 at Earth and Saturn, respectively, and scale nearly linearly with charge. The small size of t at these planets (where we note that Jupiter is about 1 order of magnitude higher) motivates a Taylor expansion of the roots. Using the expansions $\arccos(x) \approx \pi/2 - x/2$, $\cos(x) \approx 1$, and $\sin(x) \approx x$ for small x, we find

$$u_0 \approx \frac{M}{qB_0}\left[1 + \frac{qB_0}{M^3}\mu\left(1 - \frac{qB_0\omega}{\mu}\right)\right] \tag{25}$$

$$u_1 \approx \frac{\mu}{M^2}\left(1 - \frac{qB_0\omega}{\mu}\right) \tag{26}$$

$$u_2 \approx \frac{M}{2qB_0}\left[1 - 4\frac{qB_0}{M^3}\mu\left(1 - \frac{qB_0\omega}{\mu}\right)\right] \tag{27}$$

When there is no charge ($q = 0$), u_1 reduces to the familiar circular orbit radius, and the other two roots collapse to $r = 0$. For nonzero specific charge, usually $u_0 > u_2$ by about a factor of 2. We find (using the planetary magnetic properties in Table 1) that both roots u_0 and u_2 tend to be inaccessible in geocentric applications (such as in the preceding example, $u_0 \approx 0.1$ km^{-1} and $u_2 \approx 0.05$ km^{-1}), beneath the Earth's surface, and for $qB_0 < 0$ both u_0 and u_2 are negative, making them nonphysical. Further discussion of the effective potential and roots of this system is available in Grotta-Ragazzo et al. [1].

Returning to the original equations of motion [Eqs. (8–10)], we now consider perturbations around their solutions. To begin, we assign a set of generalized variables

$$\{x_1, x_2, x_3, x_4, x_5\} = \{r, \dot{r}, \theta, \dot{\theta}, \dot{\phi}\} \tag{28}$$

We denote a perturbation by $x_i + \delta x_i$, substitute into Eqs. (8–10), and neglect all nonlinear terms to obtain a set of first-order differential equations:

$$\delta\dot{x}_1 = \delta x_2 \tag{29}$$

$$\delta\dot{x}_2 = [2\mu/x_1^3 + x_5^2 + (2qB_0/x_1^3)(x_5 - \omega)]\delta x_1 + (2x_1x_5 - qB_0/x_1^2)\delta x_5 \tag{30}$$

$$\delta\dot{x}_3 = \delta x_4 \tag{31}$$

$$\delta\dot{x}_4 = -[x_5^2 + 2(qB_0/x_1^3)(x_5 - \omega)]\delta x_3 \tag{32}$$

$$\delta\dot{x}_5 = -(2x_5/x_1 - qB_0/x_1^4)\delta x_2 \tag{33}$$

Here, we have selected for the particular solution a circular equatorial orbit ($x_2 = x_4 = 0$ and $x_3 = \pi/2$), and x_1 and x_5 are the radial distance and angular velocity of the reference orbit, respectively. The out-of-plane perturbations x_3 and x_4 decouple, so that by defining

Table 1 Planetary magnetic properties

	Gravitational parameter, μ[a]	Magnetic moment, B_0[b]	Rotation period[c]
Earth	1	−1	1
Jupiter[d]	317.8	2×10^4	0.41
Saturn[d]	95.2	600	0.44

[a]Reference gravitational parameter of Earth: 398, 600 km^3/s^2.
[b]Reference dipole moment of Earth: 8×10^6 T · km^3.
[c]Reference rotation period of Earth: 24 h.
[d]Values adapted from Connerney [11].

$$\Omega_\theta^2 = x_5^2 + 2(qB_0/x_1^3)(x_5 - \omega) \tag{34}$$

we may write

$$\delta\ddot{x}_3 + \Omega_\theta^2 \delta x_3 = 0 \tag{35}$$

If $\Omega_\theta^2 > 0$, then the linearized orbit is marginally stable in small out-of-plane perturbations. That is, a perturbation will induce an oscillation of frequency Ω_θ about the equatorial plane. Similarly, one may manipulate Eqs. (29), (30), and (33) to write

$$\delta\ddot{x}_2 + \Omega_r^2 \delta x_2 = 0 \tag{36}$$

where

$$\Omega_r^2 = (2x_1x_5 - qB_0/x_1^2)(2x_5/x_1 - qB_0/x_1^4) - [2\mu/x_1^3 + x_5^2 + 2(qB_0/x_1^3)(x_5 - \omega)] \tag{37}$$

Although δx_2 corresponds to $\delta\dot{r}$ in the physical system, the stability analysis of this perturbation equation (a simple harmonic oscillator) equally applies to its integral, $\delta x_1 = \delta r$, the perturbation in position. The linearized system is marginally stable when $\Omega_r^2 > 0$, where the perturbation creates small oscillations about the reference radius x_1.

Figure 2 shows the region of marginal stability for radial and out-of-plane perturbations at Earth, using the relevant properties of Table 1. The shaded region indicates the area of marginal stability given combinations of constant specific charge and radial distance of the reference orbit, where we have assumed that the angular velocity is the equilibrium circular velocity given by Eq. (11).

The distinct asymmetry in the plots and the charge-polarity dependence of the unstable regions warrants attention. The magnetic field of the Earth is directed "upward" in the equatorial plane (i.e., from south to north), so the Lorentz force imparted on a spacecraft with a positive charge in an equatorial orbit will point radially away from the planet, opposing gravity. The magnetic field depends on the inverse cube of the radial distance from the center of the dipole, one order higher than gravity. The velocity of a free particle in orbit decreases quickly with increased distance from the center of mass (and from the center of the dipole), so that the magnetic force usually drops off more rapidly with distance than gravity. In the case of circular orbits, the velocity is proportional to $r^{-1/2}$, making the magnetic force diminish as $r^{-7/2}$, whereas gravity falls off with only r^{-2}. As specific charge increases and the Lorentz force becomes more pronounced, the force will tend to pull the spacecraft away more strongly from the planet. The angular velocity of the spacecraft decreases as it moves outward, so that the Lorentz force diminishes more quickly than gravity as the vehicle increases its radial distance. No matter what constant positive charge is chosen for a radial perturbation away from a circular orbit, the Lorentz force will always eventually pull the spacecraft away to a region where the gravitational force can reassert its dominance, keeping the spacecraft in an osculating orbit. In contrast, when the spacecraft generates a large negative charge, both gravity and the Lorentz force act in the same direction toward the center of the planet and dipole. As a perturbation directs the spacecraft toward the planet, the Lorentz force increases in strength. Further exacerbated by a growing radial velocity, the combination of gravitational and Lorentz forces applied to the spacecraft can result in instability.

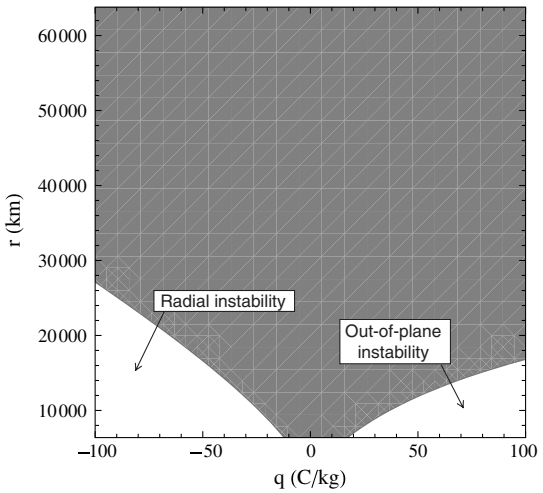

Fig. 2 Region of marginal stability (shaded) for circular orbits at a range of specific charges and orbital radii at Earth. The angular velocity for equilibrium circular orbits [derived in Eq. (11)] is assumed.

This dependence of stability on charge polarity leads to the same argument for out-of-plane perturbations. At the equatorial plane, an out-of-plane perturbation introduces a vertical component to the velocity of the spacecraft. This component, parallel to the magnetic field, creates no Lorentz force (which depends on the cross product of velocity and the field). However, the perturbation causes the spacecraft to drift slightly away from the equatorial plane, where the field is no longer exactly parallel to the velocity perturbation. The out-of-plane gradient in the magnetic field is small, which explains the orbit's relative resilience against out-of-plane perturbations. Whereas a radial perturbation may produce an unstable orbit at -10 C/kg (taken at the radius of the Earth's surface), an orbit remains stable with out-of-plane perturbations up to $+20$ C/kg. Both regions of instability are well outside the capability of near-term feasible Lorentz spacecraft.

Application to Enceladus

With the arrival of the Cassini spacecraft in the Saturnian system, the small moon Enceladus has become a source of several enticing discoveries, including the existence of liquid-water geysers near its southern pole [16]. Mission planners have given serious consideration to a flagship mission designed primarily for investigation of Enceladus. However, the design of a trajectory that maintains constant observation of the moon is a daunting challenge. Enceladus's low mass relative to Saturn often leads to instability for orbits about the moon [17,18].

We investigate a novel approach using a Lorentz spacecraft to maintain constant observation of Enceladus. Although a traditional approach would consider orbits about Enceladus proper, it is only sustained proximity to the moon that is required for long-term observation. For example, a halo orbit at a Lagrange point between Saturn and Enceladus is an attractive option for constant observation, but it too requires stationkeeping propellant, and we assume that the ostensibly stable Lagrange points L4 and L5 are too far away for useful observations. Instead, we consider a Lorentz spacecraft in orbit around Saturn. We have shown in the previous section that a Lorentz spacecraft may maintain a circular orbit about a planet at arbitrary radius and orbital velocity, given a particular specific charge. We expect that the same concept applies to the Saturn–Enceladus system, where we place the spacecraft into a circular orbit of arbitrary radius around Saturn, and choose a specific charge so that the orbital velocity is equal to that of Enceladus. As long as the power system can maintain the charge, the spacecraft can remain along the line between Saturn and Enceladus at an arbitrary observation altitude.

Figure 3 shows Saturn and Enceladus together in an isolated system (we neglect the effects of all other moons and the rings) and the two Lagrange points of interest. We will work in the rotating

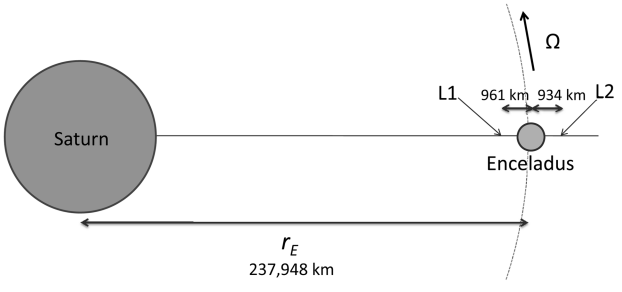

Fig. 3 Model of the Saturn–Enceladus rotating frame, not to scale.

frame throughout, so that Enceladus appears motionless with respect to Saturn. Enceladus orbits Saturn in a nearly circular orbit of radius 237,948 km every 1.37 days. We will use the same coordinates as defined in Fig. 1, where the x axis is now coincident with the Saturn–Enceladus line. The L1 Lagrange point between Saturn and Enceladus lies 236,987 km from Saturn's center, at an altitude of approximately 700 km above the surface of Enceladus. Although Enceladus is the body of interest, because we intend to explore Lorentz spacecraft orbits around Saturn and because the magnetic field is centered at Saturn, the polar coordinates will maintain their origin at Saturn's center.

Including the gravity of both Saturn and Enceladus and the magnetic field of Saturn, the Lagrangian of this system may be written

$$\begin{aligned}\mathcal{L} = {} & (\tfrac{1}{2})[\dot{r}^2 + r^2\dot{\theta}^2 + r^2(\dot{\phi}+\Omega)^2\sin^2\theta] + \mu_S/r \\ & + \mu_E(r^2 + r_E^2 - 2rr_E\cos\phi\sin\theta)^{-1/2} \\ & + (qB_0\sin^2\theta/r)(\dot{\phi}+\Omega-\omega_S)\end{aligned} \tag{38}$$

where we work now in the rotating frame of Saturn and Enceladus, introducing the additional angular velocity Ω into the ϕ-direction term of the kinetic energy and into the magnetic potential. Equation (38) leads to the equations of motion

$$\begin{aligned}0 = {} & \ddot{r} - r\dot{\theta}^2 - r(\dot{\phi}+\Omega)^2 + \frac{\mu_S}{r^2} \\ & + \mu_E\frac{r - r_E\cos\phi\sin\theta}{(r^2 + r_E^2 - 2rr_E\cos\phi\sin\theta)^{3/2}} \\ & + qB_0\frac{\sin^2\theta}{r^2}(\dot{\phi}+\Omega-\omega_S) \\ 0 = {} & r\ddot{\theta} - r\sin\theta\cos\theta(\dot{\phi}+\Omega)^2 \\ & + 2\dot{r}\,\dot{\theta} - \mu_E\frac{r_E\cos\phi\cos\theta}{(r^2 + r_E^2 - 2rr_E\cos\phi\sin\theta)^{3/2}} \\ & - 2qB_0\frac{\sin\theta\cos\theta}{r^2}(\dot{\phi}+\Omega-\omega_S) \\ 0 = {} & r\ddot{\phi} + 2\dot{r}(\dot{\phi}+\Omega) + 2r\dot{\theta}\cot\theta(\dot{\phi}+\Omega) \\ & + \frac{\mu_E r_E\sin\phi}{\sin\theta(r^2 + r_E^2 - 2rr_E\cos\phi\sin\theta)^{3/2}} - \frac{qB_0}{r^3}(\dot{r} - 2r\dot{\theta}\cot\theta)\end{aligned} \tag{39}$$

where ω_S denotes Saturn's rotational angular velocity. We note that ϕ is no longer an ignorable coordinate. It can be shown that circular equatorial orbits are a solution to these equations of motion, subject to a condition similar to Eq. (12). For this application at Enceladus, we require a Lorentz spacecraft to maintain an angular velocity of Ω, equal to the moon's orbital angular velocity, at an arbitrary radius R. The three-body analogue of Eq. (12) for this system, which is required to satisfy the equations of motion in the equatorial plane ($\theta = \pi/2$), is given by

$$q = \frac{1}{B_0(\Omega-\omega_S)}\left[R^3\Omega^2 - \mu_S - \mu_E\frac{R^2(R-r_E)}{(R^2 - 2Rr_E + r_E^2)^{3/2}}\right] \tag{40}$$

Using the values in Tables 1 and 2, we may plot q as a function of R for these equilibrium circular orbits. Figure 4 shows that the required charge is zero at two locations, at $R = 236,987$ and $R = 238,882$ km. These are the L1 and L2 Lagrange points, respectively, where we expect no charge to be required to maintain an orbit in observation of Enceladus. The asymptote in the plot corresponds to the inaccessible region below the moon's surface near its gravity well. Moving away from the Lagrange points, the required magnitude of the specific charge increases rapidly. If we prescribe no more than a few hundredths of a coulomb per kilogram as a feasible specific charge, we observe that any Lorentz spacecraft observing Enceladus must remain within approximately 100 km of either Lagrange point.

Table 2 Characteristics of Enceladus and its orbit

r_E	237,948 km
μ_E	7.2 km^3/s^2
Ω	5.307×10^{-5} s^{-1}
Physical radius	252 km

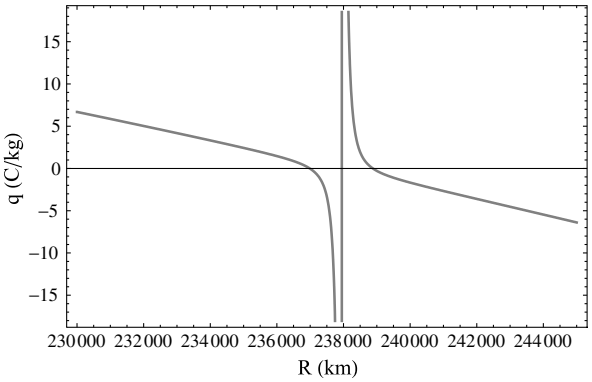

Fig. 4 The necessary constant specific charge q to maintain a circular orbit of radius R corotational with Enceladus in the Saturn–Enceladus system. The asymptote corresponds to the origin of Enceladus's gravity well.

We now consider the stability of these points with the Lorentz force included. Again, we use the set of variables

$$\{x_1, x_2, x_3, x_4, x_5, x_6\} = \{r, \dot{r}, \theta, \dot{\theta}, \phi, \dot{\phi}\} \tag{41}$$

to arrive at a set of perturbation equations. We furthermore define

$$L = \mu_E r_E x_1^{-1}(x_1^2 - 2x_1 r_E + r_E^2)^{-3/2} \tag{42}$$

$$H = \frac{3\mu_E(x_1 - r_E)^2}{(x_1^2 - 2x_1 r_E + r_E^2)^{5/2}} - \frac{x_1}{r_E}L + 2\frac{\mu_S}{x_1^3} + 2\frac{qB_0}{x_1^3}(\Omega - \omega_S) + \Omega^2 \tag{43}$$

$$J = qB_0/x_1^4 - 2\Omega/x_1 \tag{44}$$

$$K^2 = L + 2qB_0(\Omega - \omega_S)/x_1^3 + \Omega^2 \tag{45}$$

$$M = 2x_1\Omega - qB_0/x_1^2 \tag{46}$$

Denoting the perturbation by $x_i + \delta x_i$, we arrive at the linearized set of first-order equations:

$$\delta\dot{x}_1 = \delta x_2 \tag{47}$$

$$\delta\dot{x}_2 = H\delta x_1 + M\delta x_6 \tag{48}$$

$$\delta\dot{x}_3 = \delta x_4 \tag{49}$$

$$\delta\dot{x}_4 = -K^2\delta x_3 \tag{50}$$

$$\delta\dot{x}_5 = \delta x_6 \tag{51}$$

$$\delta\dot{x}_6 = L\delta x_5 + J\delta x_2 \tag{52}$$

The out-of-plane perturbations of Eqs. (49) and (50) decouple, leading to the simple harmonic oscillator $\delta\ddot{x}_3 + K^2\delta x_3 = 0$. If $K^2 > 0$, the system is marginally stable in out-of-plane perturbations. Using the physical and orbital parameters of Tables 1 and 2 and inserting Eq. (40) for q, we find that this inequality is satisfied for all $x_1 > 207,825$ km, which encompasses the L1 and L2 Lagrange

points and all other radii in the vicinity of Enceladus (the center of which is at $x_1 = r_E = 237,948$ km). The other four eigenvalues of the system are given by

$$\lambda = \pm\left(\tfrac{1}{\sqrt{2}}\right)\sqrt{H + L + JM \pm \sqrt{-4HL + (H + L + JM)^2}} \quad (53)$$

an expansion of which requires dozens of terms and therefore is not illustrative. We have found that using the equilibrium q of Eq. (40) produces eigenvalues with positive real parts in some regions along the Saturn–Enceladus line. Although there are some areas of marginal stability (i.e., where all real parts are zero), there exists a distinct region of instability near Enceladus and the Lagrange points.

This instability can, in part, be attributed to the use thus far of a constant specific charge. Near the L1 and L2 Lagrange points, where the potential has a maximum, a perturbation in either direction (toward Saturn or toward Enceladus) will give a gravitational advantage to the nearer body. Numerical integrations using the specific charge of Eq. (40) demonstrate instability in the full nonlinear regime. A constant specific charge selected through Eq. (40) for the reference orbit is not tailored to function at other radii; at the new perturbed radius, the spacecraft's Saturn-centric angular velocity will deviate from that of Enceladus, and the Lorentz spacecraft will leave the Saturn–Enceladus line.

As we wish to maintain a circular orbit about Saturn at all times so that the spacecraft keeps up with Enceladus (regardless of the radius to which a perturbation pushes the vehicle), we may consider freeing the radial coordinate in Eq. (40). However, the radial velocity acquired by a perturbation will also introduce a Lorentz force component in the ϕ direction, for which Eq. (40) alone cannot account. Instead, we heuristically introduce a tuning parameter α into Eq. (40), so that the control law for the specific charge becomes

$$q[r(t)] = \frac{\alpha}{B(\Omega - \omega_S)}\left[r(t)^3\Omega^2 - \mu_S - \mu_E\frac{r(t)^2[r(t) - r_E]}{[r(t)^2 - 2r(t)r_E + r_E^2]^{3/2}}\right] \quad (54)$$

This heuristic control depends only on the radial distance from Saturn and the tuning parameter α. To determine whether Eq. (54) is useful in stabilizing orbits, we insert the control law into the original nonlinear equations of motion [Eqs. (39)], relinearize, and calculate the new eigenvalues of the system at $x_1 = 236,987$ km, the location of the L1 Lagrange point. Excluding the out-of-plane perturbations, which still decouple as before and which still permit marginal stability near Enceladus, Fig. 5 shows a plot of the real parts of the four remaining eigenvalues as a function of α. Two of the eigenvalues are superimposed at zero on the horizontal axis. The real parts of the eigenvalues are zero for all $\alpha > 1$, implying a sort of overcompensating control for which the perturbed motion in the linearized system is marginally stable around the Lagrange point.

We propagate the full nonlinear model with the control of Eq. (54). Sample plots of the perturbed motion and plots of the specific charge

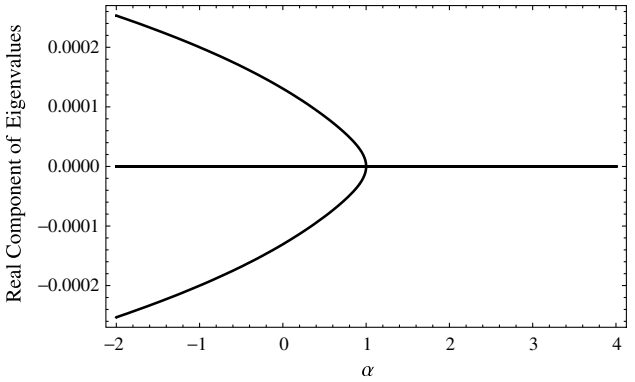

Fig. 5 The real parts of the eigenvalues (excluding decoupled out-of-plane components) of perturbed motion near the L1 Lagrange point.

and radial coordinate versus time appear in Fig. 6. Each trajectory begins with a 10 km radial offset at the Lagrange point and is disturbed by 10 m/s perturbations in the radial and along-track directions. For the case $\alpha = 1.1$, the spacecraft trajectory stays within 300 km of the L1 Lagrange point throughout the 30-day integration. Integrations for several hundred days show the same marginally stable behavior in the nonlinear regime. Increasing α constrains the trajectory in the radial direction, but the along-track deviations remain mostly unaffected. A change of α from 1.1 to 1.8 reduces the movement in the radial direction by a factor of about 2, and intermediate values of α have a more or less linear effect on the radial variations. The plots of specific charge versus time exhibit a periodic modulation of charge between approximately -0.6 and $+0.5$ C/kg for these assumed initial conditions. Higher α increases the frequency of the charge modulation. The same effect appears in the plots of radius versus time, indicating that α has a substantial role in the rate at which the spacecraft librates near L1. For illustration purposes, the trajectories of Fig. 6 were intentionally chosen to exceed the limits on feasible specific charge; near-term feasible trajectories, generated by smaller perturbations, would be too compact to easily discern the effect of α with Enceladus as a scale. We note that α has little effect on the absolute value and range of specific charge. Although trajectories that remain very close to the original reference point (the L1 Lagrange point) may be desirable from an operational perspective, effecting such a constrained orbit may require a high α and a high frequency for charge modulation, which may exceed the capabilities of the spacecraft. The frequency at which the Lorentz spacecraft can modulate its surface charge is dictated by both the hardware and the local space environment [7]. The example trajectories in Fig. 6 require a full cycle of charge polarity every 1–3 days, and we have found that values of $1.1 < \alpha < 2$ produce the lowest demands on specific charge and charge modulation. The radial position of the spacecraft with respect to Enceladus changes rapidly over these 30-day integrations, varying at approximately the same frequency as the specific charge. If the Lorentz spacecraft should lose its capability to generate charge (for example, via a hardware failure), the motion will be dictated by n-body dynamics; it will leave the Saturn–Enceladus line within a few hours and continue orbiting Saturn with occasional (and potentially deleterious) encounters with Enceladus.

We note that the motion is independent of attitude. The Lorentz spacecraft is modeled as a point charge, so that the apparent current from the vehicle always points in the direction of its velocity vector, regardless of the vehicle's orientation. The Lorentz spacecraft could maintain gross pointing on Enceladus at all times, with fine pointing determined by the vehicle's trajectory. For more feasible cases [i.e., lower specific charge than Fig. 6 (see Fig. 7)], the maximum displacement from the Lagrange point is only a few tens of kilometers, reducing the demands on active pointing.

We must also consider the maximum specific charge the Lorentz spacecraft is capable of generating, and how the size of the perturbations affect the maximum necessary charge determined by the control law. If the spacecraft's primary goal is stationkeeping at a Lagrange point (either L1 or L2, for which the dynamics are the same), we may operationally think of a perturbation as equivalent to an insertion error in position and velocity. Trajectory deviations for Lorentz spacecraft are most sensitive to velocity errors, and so we will focus on their effect on the necessary specific charge. To account for position errors, we assume a 10 km radial offset throughout.

The contours of maximum specific charge in Fig. 7 show that, considering velocity insertion errors on the order of 10 m/s (on the left side of the figure), the maximum charge required by the control law is mostly insensitive to the direction of the error. The round nature of the contours demonstrates that a radial or an along-track perturbation will require the same specific charge. For small insertion errors on the order of 1 m/s (on the right side of the figure), a velocity error in the radial direction more dramatically affects the required specific charge. Furthermore, the hatched region in the figure indicates that the contours never fall below 0.04 C/kg in this example, indicating that the presumed 10 km position error sets a floor for the maximum required charge, regardless of perturbations in velocity.

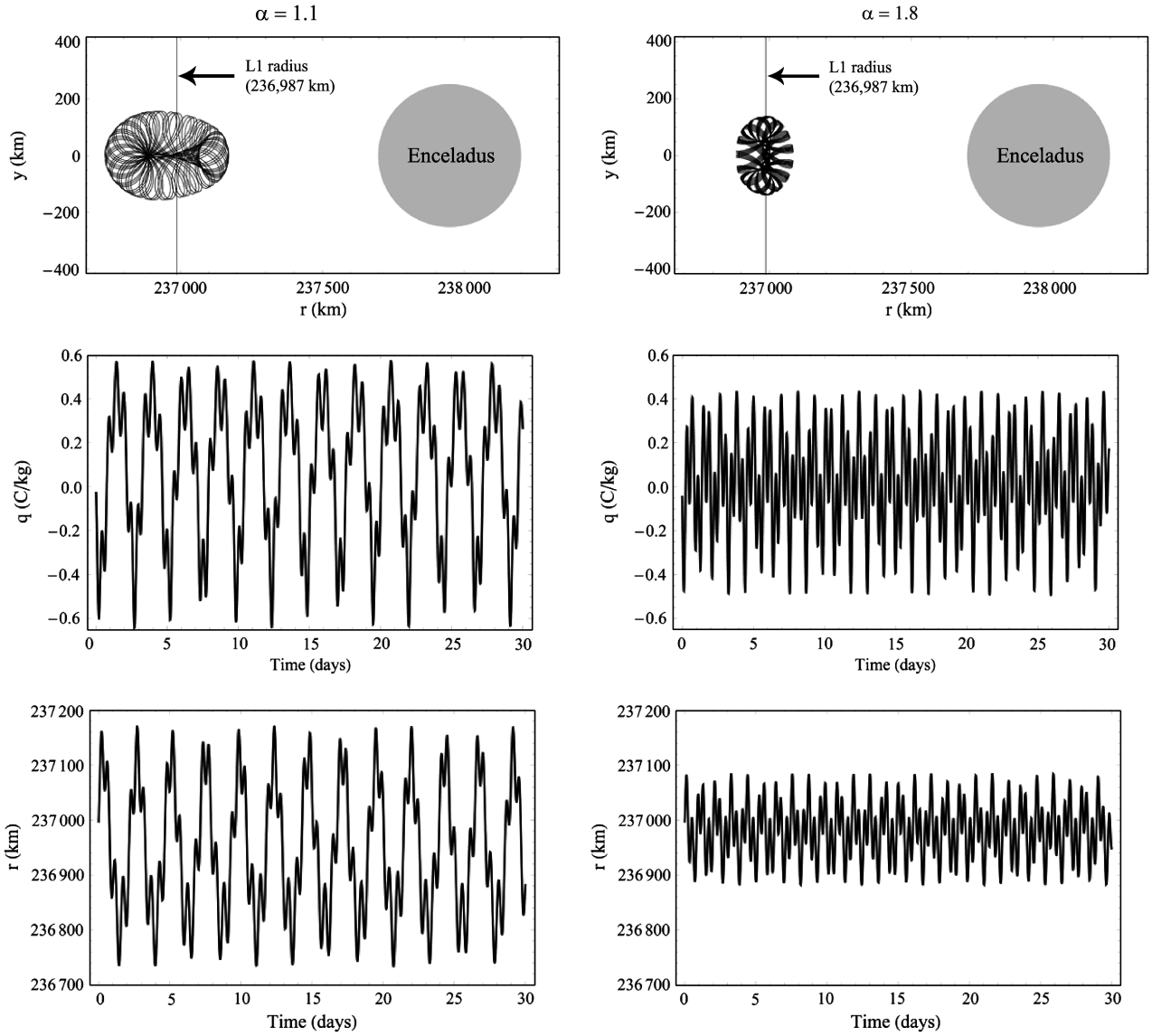

Fig. 6 Trajectories and plots of specific charge and radius versus time for two different values of α in the control law, $\alpha = 1.1$ at left and $\alpha = 1.8$ at right, integrated for 30 days. At top in the trajectory plots, the solid disk corresponds to Enceladus (to scale) and the thin vertical line marks the radial position of the L1 Lagrange point.

When this offset is removed, the contours become circular, centered at the origin, for all levels of velocity perturbations.

We have noted that the primary technological challenge for realizing a Lorentz spacecraft is charge generation, so that we wish to design a mission that requires the least specific charge. Our observation that the tuning parameter α in the control has no substantive effect on the required specific charge, but that the insertion error into L1 does (from Fig. 7), implies that navigational accuracy may be the driver for this mission's feasibility. The more accurately the Lorentz spacecraft can be inserted into L1 (or L2), the less specific charge is necessary for stationkeeping with this control. If we restrict a near-term feasible Lorentz spacecraft to around 0.05 C/kg, the contours of Fig. 7 require an insertion velocity accurate to about 1 m/s (including the presumed 10 km error in position). A position error of 10 km is consistent with the targeting errors of flybys performed by the Cassini spacecraft in orbit about Saturn [19], and the Cassini velocity errors can be as low as millimeters per second, significantly lower than the errors that the Lorentz spacecraft can tolerate for Enceladus stationkeeping.

Discussion

The heuristic control law of Eq. (54) depends only on the radial distance from Saturn and the tuning parameter α. Although operationally it may perhaps be easier to measure the distance from Enceladus, which is a solid body, an Enceladus-centered control law would be more complicated, because the magnetic field has its origin at Saturn's center. Per its derivation from the constant-velocity equilibrium charge [Eq. (40)], the control primarily affects the angular velocity of the spacecraft's orbit about Saturn. Without the tuning parameter, a Lorentz spacecraft drifting radially away from the reference orbit would gain a small along-track component of velocity (arising from the cross product of the spacecraft's new drifting radial velocity and the magnetic field). The control law with $\alpha = 1$ is insufficient to counteract the effect of this new along-track motion. The additional along-track velocity from the drift would not be accounted for, and the spacecraft would continue to move away from Enceladus. The overcompensating control introduced by the tuning parameter α drives the angular velocity of the spacecraft slightly higher or lower than Enceladus's exact orbital velocity. This adjustment to the velocity compensates for the additional along-track velocity induced by the drift away from the reference point and, by usually overcompensating, ensures a Lissajous-type orbit.

The performance of the control is recognized to be limited, in that perturbations in position or velocity can lead to large and sustained osculations about the desired orbit. We focus on this control law because it flows naturally from the equations of motion in an analytical form, which allows for substantial insight without the need

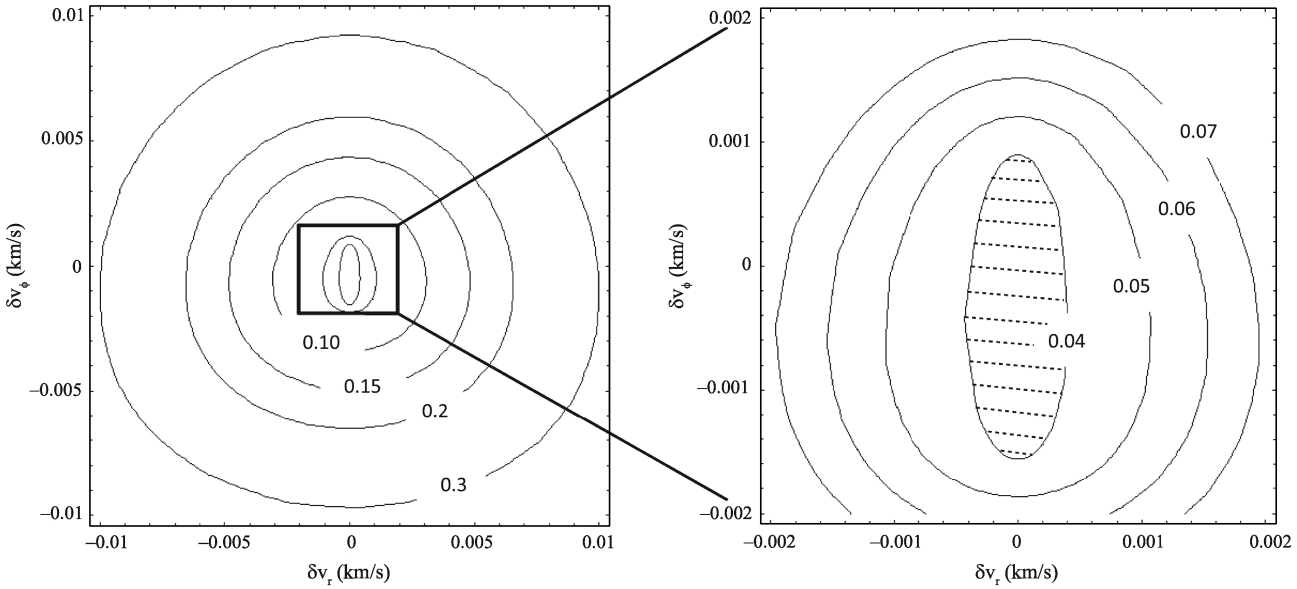

Fig. 7 Contours of maximum specific charge from the heuristic control law in Eq. (54), given perturbations (or, insertion errors) from L1 in the radial and along-track directions and including an assumed 10 km radial offset in position from L1. The labels on the contours indicate the specific charge for that contour (in units C/kg). The hatched markings on the right indicate that entire area corresponds to a 0.04 C/kg region.

for numerical computation, it involves only a single variable for state feedback (the radial distance from Saturn), and because it demonstrates overall the (marginally) stabilizing behavior we seek. We use this control as a proof of concept for this nascent technology and for this particular mission. Streetman and Peck [4] devote considerable effort to the incorporation of full state feedback control in geocentric applications to reduce the effects of a tilted dipole, but we found that their investigations still resulted in large error bounds for the Lorentz spacecraft's motion. In applications where the full state is not available, the control presented here shows that at least marginal stability is possible with radial position information alone. A more sophisticated application of feedback control (including, for example, the Lorentz spacecraft's velocity components) may, of course, improve the performance in the Saturn–Enceladus system.

Although we focus primarily on the application of the control to the L1 Lagrange point between Saturn and Enceladus, our control is equally effective at L2, beyond Enceladus, where the spacecraft is subjected to a potential about the same as at L1. Saturn's magnetic field does not change markedly over the 1400 km distance from L1 to L2. The control's usefulness at both Lagrange points is especially fortuitous, as Enceladus is tidally locked with Saturn. A Lorentz spacecraft remaining strictly at L1 views only half of the moon's surface; with a low-cost propellant maneuver or another application of the Lorentz force, the spacecraft could be transferred to L2.

If charge generation remains the primary challenge for the realization of a Lorentz spacecraft, it seems prudent to consider applications where the demand on hardware development is least severe. In the case of the heuristic control for Enceladus observation, the design element available in the control, the tuning parameter α, has little or no effect on the final amount of specific charge necessary to accomplish the mission. No choice of α made by a mission designer can mitigate (or exacerbate) the burden of charge generation. Rather, it is the magnitude of the insertion error into a Lagrange point that establishes the specific charge needs. This insertion error is determined by the limits of navigational accuracy, common to all spacecraft missions and separate from the mission design, the orbit control, and the charge generation hardware. If we restrict the spacecraft to specific charges of order 0.01 C/kg, then Fig. 7 indicates that insertion into L1 must be accomplished with no more than about 1 m/s of velocity error in the radial and along-track directions and 10 km of radial position error. Decreasing the position error widens the velocity error budget by a few meters per second. If these navigational constraints can be successfully met, a Lorentz spacecraft mission to Enceladus is (in principle) feasible in the near term.

We have not addressed a variety of other perturbing effects in the Saturnian system which may affect the behavior of a Lorentz spacecraft. Because we have worked in the equatorial plane throughout, we have neglected the oblateness of Saturn. Other gravitational forces such as Titan (the most massive Saturnian moon), Dione (a moon in resonance with Enceladus), Tethys, and Mimas were included in the nonlinear model to assess their impact. In all cases, the inclusion of these moons' gravity had no significant effect on the orbit near the Lagrange point nor on the charge generation requirements. The acceleration on the spacecraft from Titan's gravity does not exceed 9×10^{-6} m/s^2, whereas, with $q = 0.05$ C/kg, the Lorentz force accelerates the spacecraft at the Lagrange point by 5×10^{-4} m/s^2, nearly 2 orders of magnitude higher. Accelerations from Dione and Mimas are less than Titan's, and from Tethys comparable to Titan's.

Irregularities in the magnetic fields, including higher harmonics for the dipole and multipole terms, are neglected. The higher harmonics of Saturn's dipole are some 5–10% of the first harmonic, which become significant only away from the equatorial plane, and its quadrupole moment has approximately 7% of the dipole moment's strength [11]. A quadrupole moment introduces the equivalent of sectorial and tesseral harmonics to the magnetic field, disturbing motion even in the equatorial plane. Higher-fidelity analyses of the Lorentz spacecraft in the Saturnian system should take these harmonics and poles into account. Also, we note that Enceladus itself affects the shape of Saturn's magnetic field [20]. Ionized particles ejected from the moon's south pole cause the field lines to bend, deviating from a perfect dipole. Enceladus also affects the rate of rotation of the magnetic field. This nonuniformity of the field may further alter the trajectory of a Lorentz spacecraft near the Lagrange points.

Previous mission design studies for Enceladus have incorporated multibody effects and orbital resonances to maximize the viewing time of the moon [21], and a large body of literature exists on the motion of spacecraft near Lagrange points in the circular restricted three-body problem [22]. Our brief investigation of Poincaré mappings of the Saturn–Enceladus system did not immediately reveal any new limit cycles. Our first-order analysis is intended to demonstrate the existence of a propellantless option for constant observation of Enceladus given present and anticipated near-term technology. Future incorporation of multibody techniques into a higher-fidelity study may offer a variety of new options, supported by the Lorentz spacecraft's propellantless-stationkeeping capabilities.

Comparison to Other Technologies

To assess the utility of Lorentz spacecraft as an architecture for future missions, we compare its performance to electrodynamic (ED) tethers and to a traditional low-thrust system. The hardware requirements for a Lorentz spacecraft have been modeled for several applications and specific charges [4,6,8]. A Lorentz spacecraft mission that closely resembles our Enceladus stationkeeping requirements is modeled by Atchison and Peck [6], who consider the feasibility of a propellantless capture at Jupiter via the Lorentz force. The specific charge drives the sizing of the vehicle and of the power subsystem. Capture at Jupiter requires a specific charge of 0.03 C/kg, approximately the needs for stationkeeping at Enceladus. Atchison and Peck found that a Lorentz spacecraft generating 0.03 C/kg of charge and carrying 50 kg of payload requires 2 kW of power and 40 kV of electric potential. These system parameters are partially dependent on the local space environment; for our application at Saturn, where the plasma conditions are slightly more favorable for maintaining charge than at Jupiter, despite Saturn's weaker magnetic field [23], we shall assume that similar conditions hold and use this model as our reference for a Lorentz spacecraft at Saturn. We use the 50 kg payload as our baseline and consider the ratios of power and electric potential per kilogram of payload, in this case, 40 W/kg and 800 V/kg, respectively, as two figures of merit for comparison to the other two technologies. The total mass of the Lorentz spacecraft was not reported by Atchison and Peck, and the complexity of the calculation restricts us from easily reproducing the results; therefore, we use the payload mass as our metric.

The mission design for Enceladus observation may be substantially different for electrodynamic tethers or for low-thrust propulsion systems and would require its own in-depth investigation. Instead, we use for a benchmark the peak acceleration of the Lorentz spacecraft, which was found earlier to be approximately 5×10^{-4} m/s^2 given initial conditions that yield feasible specific charge, and assess how the other technologies compare in creating this acceleration.

We model an ED tether with the physical parameters given in Table 3, which are adapted from an analysis for application at Jupiter [25]. This tether is made from an aluminum ribbon. The total mass listed in Table 3 includes the mass of the tether, a 50 kg payload, and subsystem masses.

The acceleration of an ED tether is calculated from the cross product of the current and the magnetic field,

$$|\mathbf{a}| = a = |(l/m_{\text{tot}})\mathbf{I} \times \mathbf{B}| = (l/m_{\text{tot}})IB = (l/m_{\text{tot}})I(B_0/R^3) \quad (55)$$

where we assume that the current and magnetic field vectors are perpendicular in the equatorial plane of Saturn. Therefore, the current is given by

$$I = a(R^3/B_0)(m_{\text{tot}}/l) \quad (56)$$

where a is the desired acceleration, $a = 5 \times 10^{-4}$ m/s^2. The total resistance of the ribbon is given approximately by [24]

$$Z = \rho l/A \quad (57)$$

so that, to maintain this acceleration, the necessary voltage is

$$V = IZ = am_{\text{tot}}(R^3/B_0)(\rho/A) \quad (58)$$

and the necessary power is

$$P = I^2Z = a^2m_{\text{tot}}^2\rho(R^3/B_0)^2/(lA) \quad (59)$$

Insertion of the parameters of Table 3 and a, the benchmark acceleration, into Eqs. (58) and (59) yields a voltage $V = 17$ kV and a power $P = 333$ kW, or 340 V/kg and 6660 W/kg (per kilogram of payload).

Table 3 Electrodynamic tether parameters

Total mass, m_{tot}	700 kg
Length, l	50 km
Tether cross-sectional area, A	1.5 mm^2
Tether resistivity [24], ρ	2.65×10^{-8} $\Omega \cdot$ m
Orbital radius (about Saturn), R	236,987 km

For a low-thrust comparison technology, we consider the BHT-8000, manufactured by Busek [26]. The performance characteristics of the BHT-8000 appear in Table 4. The mass of the power subsystem to generate 8.3 kW is approximately 415 kg, assuming 20 W/kg with a radioisotope thermoelectric generator (RTG) [27]. Including this mass with the mass of the Hall thruster and the 50 kg payload leaves a margin of 641 kg for propellent, tanks, spacecraft structure, and other subsystems to achieve the desired acceleration of 5×10^{-4} m/s^2. With the parameters of Table 4, the low-thrust system requires 6 V/kg and 166 W/kg (per kilogram of payload).

A summary of the Lorentz spacecraft, ED tether, and Hall thruster performances appears in Table 5, where the specific power and specific voltage are measured per kilogram of payload. The lower limit on the lifetimes for Lorentz spacecraft and ED tethers are based on the approximate useful lifetime of an RTG [28]. For missions of this duration, the lifetime of the Hall thruster is limited by the erosion of the discharge chamber rather than by propellant consumption [29]. If the Hall thruster does not thrust continuously, the lifetime could be extended beyond this estimate.

In terms of power requirement, the Lorentz spacecraft, Hall thruster, and ED tether are each separated by an increasing order of magnitude, such that, on a per-kilogram-of-payload basis, the Lorentz spacecraft has the best performance. However, whereas the power requirement for the Lorentz spacecraft is optimized for a 50 kg payload, we assume that a substantial 641 kg of mass remains for the Hall thruster spacecraft, some of which may include additional payload. It is likely that the specific power for the Hall thruster could be improved (to equal or better than the Lorentz spacecraft) if the excess mass were apportioned appropriately. The performance is reversed for specific voltage, where the Hall thruster requires the least voltage to generate thrust and the Lorentz spacecraft requires the most. The main disadvantage of the Hall thruster system is its relatively short lifetime. Lorentz spacecraft and ED tethers can be powered by a variety of different means for long periods, whereas critical Hall thruster components will decay after about 10,000 h of operation. Over the timetable necessary to develop Lorentz spacecraft and ED tethers, more efficient low-thrust propulsion technology may enter the market that could negate the benefits of the other two technologies; we have chosen the BHT-8000 (which has not yet flown) as an example of low-thrust technology that also requires some research and development before being cleared for flight but has established performance characteristics.

For example, let us consider the requirements for a modest 20 kg science payload. From the values of Table 5, a Lorentz spacecraft requires 800 W and 32 kV for stationkeeping at Enceladus, whereas an ED tether vehicle would need 133 kW and 6.8 kV and a Hall thruster 3.3 kW and 120 V to create the equivalent acceleration. From these base power and voltage requirements determined via payload mass, one can (in principle) extrapolate subsystem and total spacecraft masses according to any desired model. The effect that the electric field of the Lorentz spacecraft has on the payload's ability to

Table 4 BHT-8000 Hall thruster parameters

Power	8.3 kW
Discharge voltage	300 V
Thrust	512 mN
Mass (thruster only)	20 kg

Table 5 Performance comparison[a]

	Lorentz s/c[b]	ED Tether	Hall Thruster
Specific power, W/kg	40	6660	166
Specific voltage, V/kg	800	340	6
Lifetime, yrs	10+	10+	∼1

[a]For $|a| = 5 \times 10^{-4}$ m/s^2.
[b]$q = 0.03$ C/kg.

perform field and particle science depends heavily on the nature of the experiments.

Hall thrusters have a long operational history and remain an attractive low-mass option for missions to the outer planets, and ED tethers now have a substantial pedigree in the literature and a growing record in space. Lorentz spacecraft have substantial voltage and power requirements compared to these two technologies, although this brief analysis shows that they may have some advantage in power against ED tethers and in lifetime against Hall thrusters. We also note that many suggested architectures [7–9] for a Lorentz spacecraft permit the vehicle to be modeled as a charged point mass in space, greatly reducing operational and dynamical complexity. The attitude dynamics and orbital mechanics of a multikilometer tether would be coupled in the Saturnian system, and an Enceladus mission with a Hall thruster would require constant attitude control for thrust vectoring. Compact Lorentz spacecraft may maintain station near Enceladus without a stringent need for attitude control.

Conclusions

A Lorentz spacecraft can manipulate the Lorentz force generated in a planetary magnetic field to create unconventional orbits. For a circular orbit, any two of the three parameters (specific charge, radius, and velocity) may be chosen arbitrarily, with the third determined by a simple relation. The dynamics of these circular orbits possess an analogue in a three-body system, such as when the spacecraft operates near Saturn and Enceladus. By selecting the appropriate specific charge, a Lorentz spacecraft may observe Enceladus at an arbitrary altitude while maintaining a circular orbit about Saturn with Enceladus's orbital velocity. To ensure a feasible specific charge, the Lorentz spacecraft must operate near one of the collinear Lagrange points on either side of Enceladus. A heuristic and analytical control law allows a Lorentz spacecraft to remain near the Lagrange points without propellant, using the Lorentz force from Saturn's magnetic field to (marginally) stabilize the orbit and maintain station. The feasibility of this mission is primarily affected by present-day navigational accuracy, rather than by the content of the heuristic control or mission design, and we have restricted our analysis to orbits around the Lagrange points that appear to be feasible both for Lorentz spacecraft technology and for navigation systems. Although the power and voltage requirements for a Lorentz spacecraft are considerable, in some areas the performance of Lorentz spacecraft may be comparable to or have an advantage over other technologies such as electrodynamic tethers and low-thrust propulsion systems. Considerable effort is needed to make Lorentz spacecraft a reality, but the dynamic simplicity and operational flexibility that they offer for some applications suggest that this new class of spacecraft holds promise for future space missions.

Acknowledgments

The first author is supported by a fellowship from the National Defense Science and Engineering Graduate Fellowship Program. The authors wish to thank Mason Peck of Cornell University for his encouragement to pursue this research.

References

[1] Grotta-Ragazzo, C., Kulesza, M., and Salomão, P. A. S., "Equatorial Dynamics of Charged Particles in Planetary Magnetospheres," *Physica D*, Vol. 225, No. 2, 2007, pp. 169–183. doi:10.1016/j.physd.2006.10.009

[2] Thomsen, M. F., Goertz, C. K., Northrop, T. G., and Hill, J. R., "On the Nature of Particles in Saturn's Spokes," *Geophysical Research Letters*, Vol. 9, No. 4, April 1982, pp. 423–426. doi:10.1029/GL009i004p00423

[3] Howard, J. E., Horányi, M., and Stewart, G. R., "Global Dynamics of Charged Dust Particles in Planetary Magnetospheres," *Physical Review Letters*, Vol. 83, No. 20, Nov. 1999, pp. 3993–3996. doi:10.1103/PhysRevLett.83.3993

[4] Streetman, B., and Peck, M. A., "New Synchronous Orbits Using the Geomagnetic Lorentz Force," *Journal of Guidance, Control, and Dynamics*, Vol. 30, No. 6, Nov.–Dec. 2007, pp. 1677–1690. doi:10.2514/1.29080

[5] Pollock, G. E., Gangestad, J. W., and Longuski, J. M., "Responsive Coverage Using Propellantless Satellites," AIAA Paper RS6-2008-2002, April 2008.

[6] Atchison, J. A., and Peck, M. A., "Lorentz-Augmented Jovian Orbit Insertion," *Journal of Guidance, Control, and Dynamics*, Vol. 32, No. 2, March–April 2009, pp. 418–423. doi:10.2514/1.38406

[7] Peck, M. A., "Prospects and Challenges for Lorentz-Augmented Orbits," AIAA Paper 2005-5995, Aug. 2005.

[8] Atchison, J., and Peck, M. A., "Dynamics and Feasibility of a Millimeter-Scale Lorentz-Propelled Satellite," AIAA Paper 2007-6847, Aug. 2007.

[9] Gorman, W. R., Brownridge, J. D., and Peck, M., "Experimental Study of a Lorentz Actuated Orbit," 2008, http://www.citebase.org/abstract?id=oai:arXiv.org:0805.3332.

[10] Longuski, J. M., Todd, R. E., and Koenig, W. W., "Survey of Nongravitational Forces and Space Environmental Torques: Applied to the Galileo," *Journal of Guidance, Control, and Dynamics*, Vol. 15, No. 3, May–June 1992, pp. 545–553. doi:10.2514/3.20874

[11] Connerney, J. E. P., "Magnetic Fields of the Outer Planets," *Journal of Geophysical Research*, Vol. 98, No. E10, Oct. 1993, pp. 18659–18679. doi:10.1029/93JE00980

[12] Schaub, H., Parker, G. G., and King, L. B., "Challenges and Prospects of Coulomb Spacecraft Formation Control," *Journal of the Astronautical Sciences*, Vol. 52, Nos. 1–2, Jan.–June 2004, pp. 169–193.

[13] Griffiths, D. J., *Introduction of Electrodynamics*, 3rd ed., Prentice–Hall, Upper Saddle River, NJ, 1999, pp. 202–254.

[14] Greenwood, D. T., *Classical Dynamics*, 1st ed., Dover, New York, 1997, pp. 102–146.

[15] Dullin, H. R., Horányi, M., and Howard, J. E., "Generalizations of the Störmer Problem for Dust Grain Orbits," *Physica D*, Vol. 171, No. 3, 2002, pp. 178–195. doi:10.1016/S0167-2789(02)00550-X

[16] Hansen, C. J., Esposito, L., Stewart, A. I. F., Colwell, J., Hendrix, A., Pryor, W., Shemansky, D., and West, R., "Enceladus' Water Vapor Plume," *Science*, Vol. 311, No. 5766, March 2006, pp. 1422–1425. doi:10.1126/science.1121254

[17] Russel, R. P., and Lara, M., "On the Design of an Enceladus Orbit," AIAA Paper 2008-7072, Aug. 2008.

[18] Lara, M., Palacián, J. F., and Russell, R. P., "Averaging and Mission Design: The Paradigm of an Enceladus Orbiter," American Astronautical Society Paper 09-157, Feb. 2009.

[19] Antreasian, P. G., Bordi, J. J., Criddle, K. E., Ionasescu, R., Jacobson, R. A., Jones, J. B., MacKenzie, R. A., Meek, M. C., Pelletier, F. J., Roth, D. C., Roundhill, I. M., and Stauch, J., "Cassini Orbit Determination Performance During the First Eight Orbits of the Saturn Satellite Tour," American Astronautical Society Paper 05-312, Aug. 2005.

[20] Tokar, R. L., Johnson, R. E., Hill, T. W., Pontius, D. H., Kurth, W. S., Crary, F. J., Young, D. T., Thomsen, M. F., Resienfeld, D. B., Coates, A. J., Lewis, G. R., Sittler, E. C., and Gurnett, D. A., "The Interaction of the Atmosphere of Enceladus with Saturn's Plasma," *Science*, Vol. 311, No. 5766, 2006, pp. 1409–1412. doi:10.1126/science.1121061

[21] Reh, K., "Titan and Enceladus $1B Mission Feasibility Study Report," Jet Propulsion Lab. Doc. D-37401 B, prepared for NASA's Planetary Sciences Div., Jan. 2007.

[22] Szebehely, V., "Theory of Orbits: The Restricted Problem of Three Bodies," Academic Press, New York, 1967.

[23] Streetman, B., and Peck, M. A., "Gravity-Assist Maneuvers Augmented by the Lorentz Force," AIAA Paper 2007-6846, Aug. 2007.

[24] Griffiths, D. J., *Introduction of Electrodynamics*, 3rd ed., Prentice–Hall, Upper Saddle River, NJ, 1999, pp. 286–301.

[25] Sanmartin, J. R., Charro, M., Lorenzini, E. C., Garrett, H. B., Bombardelli, C., and Bramanti, C., "Electrodynamic Tether at Jupiter, II: Fast Moon Tour After Capture," *IEEE Transactions on Plasma Science*, Vol. 37, No. 4, April 2009, pp. 620–626. doi:10.1109/TPS.2009.2013955

[26] Pote, B., Hruby, H., and Monheiser, J., "Performance of an 8 kW Hall Thruster," International Electric Propulsion Conference Paper 99-080, Oct. 1999.

[27] McDermott, J., "Power," *Space Mission Analysis and Design* edited by Larson, W. J., and Wertz, J. R., 3rd ed., Microcosm Press, El Segundo, CA, 2005, pp. 407–427.

[28] Mondt, J. F., Surampudi, S., Nesmith, B. J., and Rapp, D., "Advanced Radioisotope Power System Technology Development for NASA Missions 2011 and Beyond," ESA Paper SP-502, May 2002.

[29] Manzella, D., Yim, J., and Boyd, I., "Predicting Hall Thruster Operational Lifetime," AIAA Paper 2004-3953, Aug. 2004.